Graphitic Encapsulation of Catalyst Particles in Carbon Nanotube Production

Feng Ding,*,† Arne Rosén,† Eleanor E. B. Campbell,† Lena K. L. Falk,‡ and Kim Bolton†,§

Department of Physics, Göteborg University, SE-412 96, Göteborg, Sweden, Applied Physics, Chalmers University of Technology, SE-412 96, Göteborg, Sweden, and School of Engineering, University College of Borås, SE-50190, Borås, Sweden

Received: September 27, 2005; In Final Form: December 23, 2005

A new model is proposed for the encapsulation of catalyst metal particles by graphite layers that are obtained, for example, in low-temperature chemical vapor deposition production of carbon nanotubes (CNTs). In this model graphite layers are primarily formed from the dissolved carbon atoms in the metal−carbide particle when the particle cools. This mechanism is in good agreement with molecular dynamics simulations (which show that precipitated carbon atoms preferentially form graphite sheets instead of CNTs at low temperatures) and experimental results (e.g., encapsulated metal particles are found in low-temperature zones and CNTs in high-temperature regions of production apparatus, very small catalyst particles are generally not encapsulated, and the ratio of the number of graphitic layers to the diameter of the catalyst particle is typically 0.25 nm^{-1}).

1. Introduction

Despite the rapid progress that has been made in carbon nanotube (CNT) production since Iijima's seminal paper in 1991,[1] the detailed growth mechanism is still not known. For example, there is no known method for chiral-selective growth of single-walled carbon nanotubes (SWNTs), which has hindered the development of their applications in electronic circuitry.[2−4] Also, it is not possible to produce arbitrarily long CNTs, and catalyst particles (e.g., Fe, Co, Ni, or their alloys) are often observed to be encapsulated in graphite layers after CNT production.[5,6] Although this encapsulation may not cause the cessation of CNT growth (i.e., the graphite layers may form only once CNT growth has stopped), it is clear that encapsulation prevents the catalytic decomposition of carbon feedstock and hence poisons all active particles.[5]

Fe, Co, and Ni particles that are encapsulated in graphitic layers are also important magnetic materials,[7,8] which, due to their unique magnetic properties and high physical and chemical stability, have potential applications in high-density magnetic recording media.[9−12] Controlling the size of the magnetic nanoparticles and the thickness of the encapsulating graphitic layers is critical for designing this type of recording media.

In addition to its importance for data storage and its possible role in the poisoning of catalyst particles during CNT growth, understanding the mechanism of transition-metal particle encapsulation in graphite sheets may also shed light on the growth mechanism of CNTs. For example, the concentration and location of carbon atoms in catalyst particles depends on the phase of the particles, which, in turn, depends on the growth temperature and particle size. The model proposed here relates the number of graphite layers that are observed after CNT growth to the concentration of dissolved carbon atoms, which yields information on the composition of the metal−carbide particle during growth.

* To whom correspondence should be addressed. Tel: +1-713-348-5657. E-mail: feng.ding@rice.edu.
† Göteborg University.
‡ Chalmers University of Technology.
§ University College of Borås.

2. Encapsulation of Metal Particles

Before presenting the model for the graphitic encapsulation of metal particles, we briefly summarize key experimental and computational results that are important to the model.

2.1. Key Experimental Results. Experimental observations of the encapsulation of catalyst particles include:

A. Very small catalyst particles (<2 nm) are not encapsulated,[13,14] whereas larger particles are surrounded by one or more graphite layers.

B. The major carbon byproduct for most CNT production methods is amorphous carbon. Of relevance to this work is that, in contrast to this amorphous material, graphitic structures are only observed on the surface of metal particles (amorphous carbon is often observed on the outer surface of these graphitic layers).[15,16] The fact that graphite sheets are observed on catalyst particle surfaces only, indicates that the catalyst is involved in the growth of the graphitic layers.

C. Although both pure metal and metal carbide particles can be encapsulated, in many cases it is only encapsulated pure metal particles that are observed. As reported by Zhang et al.,[17] the encapsulated core can be α-Fe or a coexistence of α-Fe and Fe_3C, but in this paper, none of the Fe_3C particles were observed to be encapsulated with graphitic shells.

D. In catalyzed carbon vapor deposition (CCVD) experiments, CNTs are found in the high-temperature zone (∼1261 K) of the oven, whereas encapsulated catalyst particles are found in low-temperature regions (<898 K).[18] This indicates that the temperature plays an important role in determining the branching ratio between CNT formation and particle encapsulation.

E. The ratio of the number of encapsulating graphitic layers, N, to the particle diameter, D, is typically 0.2−0.3 nm^{-1}. For example, Figure 1 is a high-resolution transmission electron microscope image showing catalyst particle encapsulation from CCVD growth.[14] Although a few particles are encapsulated by very many layers (e.g., a 7-nm particle encapsulated by six layers was observed in ref 14), the vast majority yield $N/D \approx 0.3$ nm^{-1}. For example, the 10-nm particle in the upper left of the image

10.1021/jp055485y CCC: $30.25
Published on Web 03/24/2006

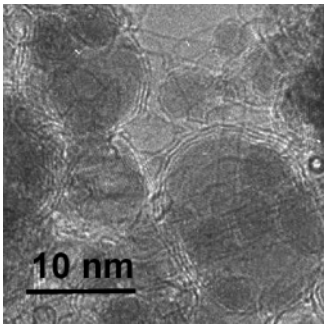

Figure 1. High-resolution transmission electron microscope image of graphitic encapsulation of metal catalyst particles after CCVD CNT growth. The ratio of the number of graphitic layers to the particle diameter is ~0.3 nm^{-1}.

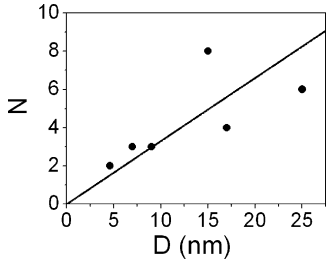

Figure 2. Number of graphite layers, *N*, vs particle diameter, *D*, obtained from arc discharge experiments of CNT growth presented in ref 19. The slope of the straight line fit, *N*/*D*, is 0.3 nm^{-1}.

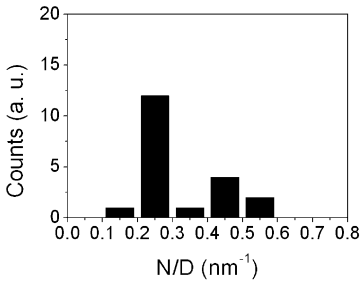

Figure 3. Histogram of *N*/*D* for the data in Figure 2 and for low-temperature formation of graphitic covered magnetic nanoparticles (see text). Over half of the data yield 0.2 < *N*/*D* < 0.3 nm^{-1}.

is encapsulated in ~3 graphite layers, the 13-nm particle in the lower right by ~4 layers and many of the smaller particles by 1−2 layers.

The number of graphitic layers vs particle diameter shown in Figure 2 is taken from ref 19, where arc discharge is used for CNT production. Here the slope of the straight line fit through the data is $N/D = 0.3\ nm^{-1}$.

Similar values for *N*/*D* are observed when graphitic layer encapsulated magnetic particles (Fe, Co, Ni) are produced at low temperatures. Typical examples are presented in ref 20 ($D = 10$ nm, $N = 3$; $D = 9$ nm, $N = 4$; $D = 14$ nm, $N = 2$; $D = 17$ nm, $N = 5$) and ref 21 ($D = 10$ nm, $N = 3$; $D = 11$ nm, $N = 5$; $D = 15$ nm, $N = 4$; $D = 10$ nm, $N = 3$; $D = 12$ nm, $N = 3$; $D = 7$ nm, $N = 4$; $D = 19$ nm, $N = 4$). These data, together with that presented in Figure 2, are shown in Figure 3. Over half of the data yield 0.2 < *N*/*D* < 0.3 nm^{-1} and all are smaller than 0.6 nm^{-1} (the second peak in this bimodal distribution, 0.3 < *N*/*D* < 0.6 nm^{-1}, is discussed below). This is in sharp contrast to the very thick graphitic layers that encapsulate metal particles produced at high temperatures, where *N*/*D* can be as large as 2.0 nm^{-1} (e.g., Saito has reported a 9-layer encapsulated 5-nm particle from catalytic arc discharge method,[22] and Harris and Tsang reported a 33-layer encapsulated 17-nm molybdenum particle produced by 2000 °C thermal annealing[23]).

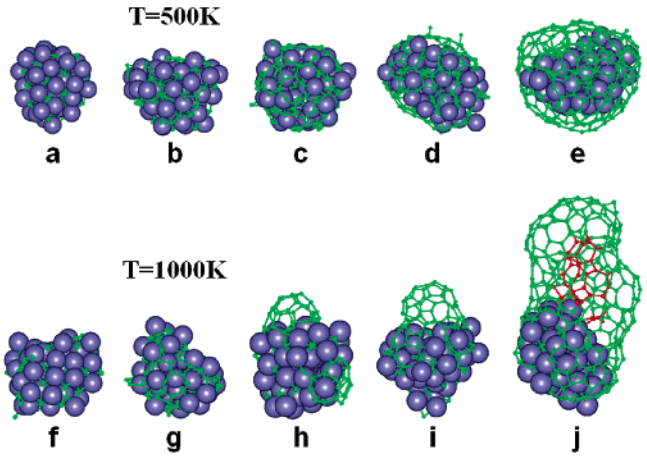

Figure 4. Snapshots from typical MD simulations of iron-catalyzed formation of carbon species at 500 K (a−e) and 1000 K (f−j). At low temperatures (<700 K), the particle is encapsulated by a graphitic layer whereas SWNTs are nucleated at intermediate temperatures (between 800 and 1400 K). Carbon atoms are shown as ball-and-stick and Fe as large spheres. Carbon atoms (defects) that occur on the inside of the SWNT are shown in red (j).

2.1. Computational Results. Molecular dynamics (MD) simulations have been used to understand the influence of temperature on the catalytic growth of carbon species from small iron particles.[24−27] In particular, dissolving of carbon into the iron particle as well as their subsequent precipitation onto the particle surface and formation of solid carbon species was studied at low (500−800 K), intermediate (800−1400 K), and high (>1400 K) temperatures.

Figure 4 shows snapshots from typical trajectories at low and intermediate temperatures (at high temperature carbon soot is formed). For both temperatures, the nucleation of carbon species begins by precipitation of carbon atoms on the particle surface. These atoms form short carbon strings (panels b and f) that grow into carbon polygons and islands (panels c and g). These islands increase in diameter and, depending on the temperature, encapsulate the iron particle or form a SWNT. When the temperature is lower than 700 K, the kinetic energy is not sufficient to overcome the attraction between the island and the metal particle, and the island thus remains on the surface and increases in size until the particle is completely encapsulated (panel e). At temperatures higher than 800 K, the kinetic energy is sufficient to overcome the attraction between the island and the metal particle so that the island lifts off the surface to form a graphitic cap (panel h). At temperatures between 800 and 1400 K, this cap grows in diameter and length to form a SWNT (panels i and j).

The MD results are in agreement with thermodynamic theory,[28,29] which also reveal the influence of kinetic energy on the branching ratio between particle encapsulation and SWNT formation. In addition, these results agree with experimental observations that encapsulated particles are formed at low temperature and CNTs at higher temperature.[18]

2.3. Model of Particle Encapsulation. Both the experimental and theoretical results discussed above indicate that particle encapsulation occurs only at sufficiently low temperatures. The transition from CNT growth to particle encapsulation may thus occur as the particle cools, or as the particle size—and hence melting point—increases. The MD simulations show that, during the growth of the first (outer) sheet, precipitating carbon atoms join to the edge of the sheet rather than precipitating between

Figure 5. Illustration of the layer-by-layer encapsulation mechanism of catalyst particles. Atoms in the outer layers (a and b) may arise directly from carbon feedstock decomposition near the edge of the growing layer or from the precipitation of atoms in the metal-carbide particle, whereas atoms in the inner layers (c−e) originate from the metal−carbide.

the sheet and the cluster (since carbon bonding at the edge of the growing sheet is far more exothermic than precipitation under an existing graphite layer). Hence, encapsulation of the particle by a single graphitic sheet precedes the formation of additional layers. Also, the proximity of the graphite sheets to the catalyst particles, observed in experiments, indicates that the particles act as substrates for the formation of the sheets. This means that, after the formation of the first sheet, the additional graphitic layers form between this sheet and the particle. Since the first sheet, which may be formed from the dissolved carbon atoms that precipitate to the surface and/or by decomposition of feedstock near the edge of the growing sheet, covers the entire particle and prevents further catalytic decomposition, all successive (inner) layers are formed from dissolved carbon atoms only. This is supported by the experimental observation that encapsulated particles are often pure metal (or a combination of pure metal and carbide) and metal carbide particles are often observed without encapsulation.[17]

Figure 5 illustrates our model for multilayer encapsulation of metal particles, where we assume that the outer layer is complete (panels a and b) before inner layers are formed (panel c). The model does not stipulate if the atoms in the outer sheet arise directly from carbon feedstock decomposition—where atoms join to the growing graphite sheet without dissolving into the cluster—or from precipitation of atoms from the metal−carbide particle, but to simplify the analysis presented below we assume that all atoms (in all sheets) arise from the precipitation of dissolved carbon atoms. This assumption is also based on the fact that small particles are not encapsulated[13,14] (i.e., they can also decompose feedstock but, as discussed below, do not contain a sufficient number of dissolved atoms to form a graphite layer).

The model illustrated in Figure 5 can also be understood in terms of bulk metal and metal−carbide thermodynamics, where it is well known that metal carbides are stable at high temperatures (e.g., M_3C is the most stable structure for M = Fe, Co, and Ni), and upon cooling, they undergo a phase transition to metal−carbide alloys with very low carbon concentrations and graphite.[9,21,30] For example, the carbon content of bulk Fe_3C phase is 6.7% in weight, and this decreases to lower than 0.022% for α iron at temperatures lower than 1000 K. Ni and Co have very similar phase diagrams and are expected to exhibit the same behavior.

By assumption, as discussed above, that all atoms in the graphite sheets arise from carbon atoms in the metal-carbide particles and that the particle composition is not strongly dependent on its size, then the number of graphite sheets, N, is proportional to the number of carbon atoms that are originally in the particle and hence the particle diameter, D. In particular, the surface area of a spherical cluster with diameter D, which is similar to the area of the graphite sheets that encapsulate it, is $S = \pi D^2$. The average area of each atom in the graphite hexagonal geometry is $S_C = 1.5(3)^{1/2} d_{C-C}^2$, where $d_{C-C} = 1.42$ Å is the C−C bond length. Hence, the number of carbon atoms required to form each encapsulating graphite layer is approximately $N_C = S/S_C = 1.209D/d_{C-C}^2$.

These N_C atoms originate from a metal−carbide particle, where the carbon:metal atom ratio before formation of the graphite layers is denoted by α and after encapsulation by β. Since the number of metal atoms in a cluster of diameter D is $N_M = 1/6\pi D^3\rho$, where ρ is the metal atom density (0.141 mol/cm^3 for bulk iron), the number of graphitic layers deposited on the particle is

$$N = \frac{(\alpha - \beta)N_M}{N_C} = 0.433(\alpha - \beta)D d^2_{C-C}\rho$$

Insertion of $\alpha = 0.33$, since the M_3C phase is stable for M = Fe, Ni, and Co at high temperatures, and $\beta = 0.0$, since encapsulated particles can be pure (or almost pure) metal, yields

$$\frac{N}{D} = 0.25\ (\mathrm{nm}^{-1})$$

The corresponding ratios of $N/D = 0.26$ and 0.27 nm^{-1} were obtained for Co and Ni, respectively.

These ratios are very similar to the experimental data presented above and strongly support the proposed model. In addition, the experimental observation that small catalyst particles ($D < 2$ nm) are not encapsulated also supports the model since the number of atoms in particles of this size are too few to form a complete graphitic layer (i.e., when $D < 2$ nm then $N \approx (0.25-0.27)D < 0.6$).

It is important to note that, depending on their size, the carbon concentration in catalyst particles at high temperatures may be larger than the metastable M_3C discussed above. For example, Fe_7C_3[31] has been observed after CNT growth from small Fe particles. This will increase the ratio of the number of encapsulated layers to the catalyst particle diameter. Also, it has been observed that the core of large encapsulated particles may have low carbon concentrations,[17] and the number of the encapsulated graphitic layers will be less than that predicated by the model.

3. Discussion

3.1. Comparison with Other Models. Models of the encapsulation of catalyst particles include the growth mechanism for carbon onions, the metal−carbon liquid drop mechanism, models for the preferential growth of encapsulating graphite layers vs SWNTs for large catalyst particle, and the dissolve−diffusion−precipitation (DDP) model. Carbon onions are often produced under experimental conditions that are very different from those used when growing CNTs (e.g., onions are produced using ion and electron irradiation of small carbon clusters,[32,33] thermal annealing of very small diamond particles[34] or arc discharge in water[35]), and the metal−carbon liquid drop mechanism is only applicable for very high temperature nucleation where the dissolved carbon concentration is high and the metal is in the liquid state (e.g., arc discharge experiments).[22,36] Under these high-temperature conditions, very thick graphitic layers can form on the catalyst particle surface (e.g., N/D can be greater than 2 in some arc discharge experiments[22]). Hence we limit the comparison of our model with those that describe the preferential encapsulation of large catalyst particles and the DDP model.

3.1.1. Models for the Preferential Encapsulation of Large Catalyst Particles. It has been proposed that graphitic encapsulation of metal particles is thermodynamically preferred to SWNT growth when the particle diameter is larger than 3 nm.[13]

This explained observations in earlier experiments that SWNTs form only on clusters with small diameters (about 1−2 nm). Although this model is sufficient to explain these observations, it does not describe the formation of multilayer graphitic shells. In addition, more recent experiments reveal that, depending on growth conditions, multiwall carbon nanotube (MWNT) growth can be preferred to particle encapsulation for large catalyst particles,[37] and large-diameter SWNTs (>5 nm) can also be grown.[38,39] Although this model has some similarities to the one presented here, it does not consider the key role of the temperature on the branching ratio between CNT growth and particle encapsulation.

3.1.2. DDP Model. The DDP mechanism,[40,41] which is similar to the vapor−liquid−solid (VLS) model for CNT growth,[22] assumes that the carbon atoms dissolve into the catalyst particle, and when the particle is highly supersaturated in carbon, these atoms precipitate on the surface and form graphitic layers. This model is similar to the one proposed here and can explain the nucleation of graphitic layers on the catalytic metal surface at lower temperatures (e.g., 600 °C).[42] However, the model presented here explicitly predicts the number of graphite layers that are formed from particles of differing sizes.

3.2. Composition of Metal−Carbide Catalysts during CNT Growth. The carbon concentration of metal−carbide catalyst particles plays an important role during the nucleation and growth of CNTs. In situ measurements of this concentration are not possible, and the model proposed here provides a simple estimation of the catalyst particle carbon mol fraction during CNT growth. That is, if one assumes that the particles that are encapsulated are the same as those that grow CNTs, or if one assumes that particles that grow CNTs have the same carbon content as those that become encapsulated, then the carbon atoms that form the encapsulating graphite layers provide an estimate of the number of dissolved carbon atoms during CNT growth (or just before growth stops and the cluster is encapsulated). As discussed above, if all carbon atoms in the encapsulating layers are originally dissolved in the metal−carbide particle and the encapsulated particle is pure metal (all dissolved carbon atoms precipitate and form graphite sheets), this yields a composition close to M_3C, where M is Fe, Co, or Ni. Encapsulated carbide particles, or particles that are surrounded by many layers (e.g., the second peak in the bimodal distribution in Figure 3), can be formed if the carbon content during CNT growth is larger than M_3C (e.g., it may be another metal−carbide species such as Fe_7C_3) or if the first graphite sheet does not completely encapsulate and poison the catalytic particle. The latter possibility could occur if there are large defects in the graphite sheet or if other atoms that are bonded to the cluster surface (e.g., substrate or alloying species) prevent complete encapsulation.

3.3. Poisoning of Catalyst Particles. Although the mechanism of catalyst particle poisoning at the end of CNT growth is still under debate, it is clear that the encapsulation of particles prevents further feedstock decomposition and hence CNT growth. Active particles are thus not encapsulated and, according to the model presented here, encapsulation can be reduced by maintaining elevated temperatures. This is in agreement with experimental results that high CNT yields are obtained at high temperatures.[43]

4. Conclusion

A new model for the graphitic encapsulation of catalyst metal particles is proposed. Carbon atoms that are dissolved in the metal−carbide particle precipitate on the particle surface, and at sufficiently low temperatures, graphitic layers are formed (instead of CNTs). Encapsulation dominates over CNT growth since the kinetic energy at these temperatures is not sufficient for graphitic islands to lift off the particle surface. On the basis of experimental results showing that predominantly pure (non-carbide) particles are encapsulated, it is assumed that all dissolved carbon atoms precipitate into graphitic layers. Hence, by measurement of the number of graphite layers (which gives the number of carbon atoms originally dissolved in the metal−carbide) and the particle diameter, one can estimate that the metal−carbide composition before encapsulation is typically M_3C (M = Fe, Co, or Ni). Since small catalyst particles ($D <$ 2 nm) do not contain a sufficient number of carbon atoms to form a complete graphite layer, they are free of encapsulation. The proposed mechanism is also relevant for low-temperature synthesis of graphite layers on magnetic nanoparticles.

Acknowledgment. The authors acknowledge Dr. R. Morjan for fruitful discussion. We are grateful to the Swedish Foundation for Strategic Research (CARAMEL consortium) and the Swedish Research Council for financial support and for time allocated on the Swedish National Supercomputing facilities.

References and Notes

(1) Iijima, S. *Nature* **1991**, *354*, 56.
(2) Bellucci, S. *Phys. Stat. Sol. C* **2005**, *2*, 34.
(3) Ajayan, P. M.; Ebbesen, T. W. *Rep. Prog. Phys.* **1997**, *60*, 1025.
(4) Odom, T. W.; Huang, J.-L.; Kim, P.; Lieber, C. M. *J. Phys. Chem. B* **2000**, *104*, 2794.
(5) Ci, L.; Rao, Z.; Zhou, Z.; Tang, D.; Yan, X.; Liang, Y.; Liu, D.; Yuan, H.; Zhou, W.; Wang, G.; Liu, W.; Xie, S. *Chem. Phys. Lett.* **2002**, *359*, 63.
(6) Liu, B. H.; Ding, J.; Zhong, Z. Y.; Dong, Z. L.; White T.; Lin, J. Y. *Chem. Phys. Lett.* **2002**, *358*, 96.
(7) Teunissen, W.; Groot, F. M. F. De; Geus, J.; Stephan, O.; Tence, M.; Colliex, C. *J. Catalyst* **2001**, *204*, 169.
(8) Gadd, G. E.; Collela, M.; Blackford, M.; Dixon, A.; Evans, P. J.; McCulloch, D.; Bullcock, S.; Cockayne, D. *Carbon* **2001**, *39*, 1769.
(9) Host, J. J.; Block, J. A.; Parvin, K.; Dravid, V. P.; Alpers, J. L.; Sezen, T.; LaDuca, R. *J. App. Phys.* **1997**, *83*, 793.
(10) Scott, J. H.; Majetich, S. *Phys. Rev. B* **1995**, *52*, 12564.
(11) Yogi, T.; Nguyen, T. *IEEE Trans. Magn.* **1993**, *29*, 307.
(12) Rana, R. K.; Brukental, I.; Yeshurun, Y.; Gedanken, A. *J. Mater. Chem.* **2003**, *13*, 663.
(13) Hafner, J. H.; Bronikowski, M. J.; Azamian, B. R.; Nikolaev, P.; Rinzler, A. G.; Colbert, D. T.; Smith, K. A.; Smalley, R. E. *Chem. Phys. Lett.* **1998**, *296*, 195.
(14) Bladh, K.; Falk, L. K. L.; Rohmund, F. *Appl. Phys. A* **2000**, *70*, 317.
(15) Demoncy, N.; Stephan, O.; Brun, N.; Colliex, C.; Loiseau, A.; Pascard, H. *Eur. Phys. J. B* **1998**, *4*, 147.
(16) Wang, Z. H.; Choi, C. J.; Kim, B. K.; Kim, J. C.; Zhang, Z. D. *Carbon* **2003**, *40*, 1751.
(17) Zhang, Z. D.; Zheng, J. G.; Skorvanek, I.; Wen, G. H.; Kovac, J.; Wang, F. W.; Yu, J. L.; Li, Z. J.; Dong, X. L.; Jin, S. R.; Liu W.; Zhang, X. X. *J. Phys.: Condens. Matter* **2001**, *13*, 1921.
(18) Sano, N.; Akazawa, H.; Kikuchi, T.; Kanki, T. *Carbon* **2003**, *41*, 2159.
(19) Gavillet, J.; Thibault, J.; Stephan, O.; Amara, H.; Loiseau, A.; Bichara, Ch; Gaspard, J.-P.; Ducastelle F. *J. Nanosci. Nanotechnol.* **2004**, *4*, 346.
(20) Flahaut, E.; Agnoli, F.; Sloan, J.; O'Connor, C.; Green, M. L. H. *Chem. Mater.* **2002**, *14*, 2553.
(21) Jiao J.; Seraphin, S.; Wang X.; Withers, J. C. *J. Appl. Phys.* **1996**, *80*, 103.
(22) Saito, Y. *Carbon* **1995**, *33*, 979.
(23) Harris P. J. F.; Tsang, S. C. *Chem. Phys. Lett.* **1998**, *293*, 53.
(24) Ding, F.; Bolton, K., Rosén, A. *J. Phys. Chem. B* **2004**, *108*, 17369.
(25) Ding, F.; Rosén, A.; Bolton, K. *Chem. Phys. Lett.* **2004**, *393*, 309.
(26) Ding, F.; Rosén, A.; Bolton, K. *J. Chem. Phys.* **2004**, *121*, 2775.
(27) Ding, F.; Rosén, A.; Bolton, K. *Carbon* **2005**, *43*, 2215.
(28) Kanzow, H.; Ding, A. *Phys. Rev. B* **1999**, *60*, 11180.
(29) Kanzow, H.; Lenski, C.; Ding, A. *Phys. Rev. B* **2001**, *63*, 125402.

(30) Ruskv, T.; Asenov, S.; Spirov, I.; Garcia, C.; Mönch, I.; Graff, A.; Kozhuharova, R.; Leonhardt, A.; Muhl, T.; Ritschel, M. *J. Appl. Phys.* **2004**, *96*, 7514.

(31) Yao, Y.; Falk, L. K. L.; Morjan, R.; Nerushev O. A.; Campbell E. E. B. *J. Mater. Sci.: Mater. Elec.* **2004**, *15*, 533.

(32) Ugarte, D. *Nature* **1992**, *359*, 707.

(33) Thune, E.; Cabioch, Th.; Jaouen, M.; Bodart, F. *Phys. Rev. B* **2003**, *68*, 115434.

(34) Kuznetsov, V. L.; Chuvilin, A. L.; Butenko, Y. V.; Malkov, Y. V.; Titov, V. M. *Chem. Phys. Lett.* **1994**, *222*, 343.

(35) Sano, N.; Wang, H.; Chhowalla, M.; Alexandrou, I.; Amaratunga, G. A. J. *Nature* **2001**, *414*, 506.

(36) Saito, Y.; Okuda, M.; Yoshikawa, T.; Kasuya A.; Nishina, Y. *J. Phys. Chem.* **1994**, *98*, 6696.

(37) Rao, C. N. R.; Kulkarni, G. U.; Govindaraj, A.; Satishkumar, B. C.; Thomas, P. J. *Pure Appl. Chem.* **2000**, *72*, 21.

(38) Cheung, C. L.; Kurtz, A.; Park, H.; Lieber, C. M. *J. Phys. Chem. B* **2002**, *106*, 2429.

(39) Lebedkin, S.; Schweiss, P.; Renker, B.; Malik, S. *Carbon* **2002**, *40*, 417.

(40) Jiao, J.; Seraphin, S. *J. Appl. Phys.* **1998**, *83*, 2442.

(41) Babonneau, D.; Cabioch, T.; Naudon, A.; Girard. J. C.; Denanot, M. F. *Surf. Sci.* **1998**, *409*, 2442.

(42) Tomita, S.; Hikita, M.; Fujii, M.; Hayashi, S.; Yamamoto. K. *Chem. Phys. Lett.* **2000**, *316*, 361.

(43) Bronikowski, M. J.; Willis, P. A.; Colbert, D. T.; Smith, K. A.; Smalley, R. E. *J. Vac. Sci. Technol. A* **2001**, *19*, 1800.